

Space-Time Clustering and Correlations of Major Earthquakes

James R. Holliday,^{1,2,*} John B. Rundle,^{1,2,3,†} Donald L. Turcotte,^{3,‡} William Klein,^{4,§} and Kristy F. Tiampo^{5,¶}

¹Center for Computational Science and Engineering, University of California, Davis

²Department of Physics, University of California, Davis

³Department of Geology, University of California, Davis

⁴Department of Physics, Boston University

⁵Department of Earth Sciences, University of Western Ontario, Canada

(Dated: February 1, 2022)

Earthquake occurrence in nature is thought to result from correlated elastic stresses, leading to clustering in space and time. We show that occurrence of major earthquakes in California correlates with time intervals when fluctuations in small earthquakes are suppressed relative to the long term average. We estimate a probability of less than 1% that this coincidence is due to random clustering.

INTRODUCTION

It is widely accepted [1, 2, 3, 4, 5, 6, 7, 8, 9, 10, 11] that the observed earthquake scaling laws indicate the existence of phenomena closely associated with proximity of the system to a critical point. More specifically, it has been proposed that earthquake dynamics are associated either with a second order critical point [3, 4, 5, 6, 7, 8, 11] or a mean field spinodal [9, 10] that can be understood as a line of critical points. Mean field theories of the Ginzburg-Landau type have been proposed [7, 8, 9, 10] to explain the phenomenology associated with scaling and nucleation processes of earthquakes, which would in turn imply that a Ginzburg criterion is applicable [12]. If mean field Ginzburg-Landau equations do describe earthquakes, the dynamics must be operating outside the critical region, and fluctuations are correspondingly reduced.

To summarize our results

We compare the performance of two probability measures that define the locations of future earthquake occurrence: the spatially coarse-grained seismic *intensity* and the *intensity change*. We show that an order parameter $\Psi_I(t)$ can be defined based on the performance of these probability measures on a *Receiver Operating Characteristic* (ROC) diagram and that a generalized Ginzburg criterion $\mathcal{G}(t)$ can be established measuring the relative importance of fluctuations in $\Psi_I(t)$. We find that since 1960, major earthquakes in California with magnitudes $m \geq 6$ tend to preferentially occur during intervals of time when $\mathcal{G}(t) < 1$, consistent with mean field dynamics. Currently in northern California, $\mathcal{G}(t) < 1$.

tudes -124°E and -115°E , coarse-grained in time intervals of one day. Only events above a magnitude threshold $m_T \geq 3$ are used to ensure catalog completeness. Figure 1 shows the event locations. We tile the region with a spatially coarse-grained mesh of N boxes, or pixels, having side length 0.1° , about 11 km at these latitudes, approximately the rupture length of an $m \sim 6$ earthquake. The average intensity of activity $I(\mathbf{x}, t_0, t_2)$ is constructed by computing the number of earthquakes $n(\mathbf{x}, t_0, t_2)$ in each coarse-grained box centered at \mathbf{x} since records began at time $t_0 = 1932$ until a later time t_2 that will be allowed to vary: $I(\mathbf{x}, t_0, t_2) = n(\mathbf{x}, t_0, t_2)$. We then regard $P_\mu \equiv P_\mu(\mathbf{x}, t_0, t_2) = I(\mathbf{x}, t_0, t_2) / \int I(\mathbf{x}, t_0, t_2) d\mathbf{x}$ as a probability for the location of future events $m \geq m_T$ for times $t > t_2$. Previous work [13, 14, 15] indicates that P_μ is a good predictor of locations for future large events having $m \geq 5$.

The intensity change map builds upon the intensity map by computing the average squared change in intensity over a time interval $\Delta t = t_2 - t_1$. Here we use $\Delta t = 13$ years [13, 14]. We compute $n(\mathbf{x}, t_b, t_1)$ and $n(\mathbf{x}, t_b, t_2)$ for the two times t_1 and t_2 , where $t_2 > t_1$, beginning at a base time t_b , where $t_1 > t_b > t_0$. Computing the change in numbers of events as $\Delta n(\mathbf{x}, t_b, t_1, t_2) = n(\mathbf{x}, t_b, t_2) - n(\mathbf{x}, t_b, t_1)$, we then define the intensity change $\Delta I(\mathbf{x}, t_1, t_2)$ by normalizing $\Delta n(\mathbf{x}, t_b, t_1, t_2)$ to have spatial mean zero and unit variance, yielding $\Delta n'(\mathbf{x}, t_b, t_1, t_2)$, and then averaging $\Delta n'(\mathbf{x}, t_b, t_1, t_2)$ over all values for t_b from t_0 to t_1 : $\Delta I(\mathbf{x}, t_1, t_2) = \langle \Delta n'(\mathbf{x}, t_b, t_1, t_2) \rangle_{t_b}$. The corresponding probability is $P_\Delta \equiv P_\Delta(\mathbf{x}, t_1, t_2) = [\Delta I(\mathbf{x}, t_1, t_2)]^2 / \int [\Delta I(\mathbf{x}, t_1, t_2)]^2 d\mathbf{x}$. Previous work [13, 14, 15] has found that P_Δ is also a good predictor of locations for future large events having $m \geq 5$. P_Δ can be viewed as a probability based upon the squared change in intensity.

INTENSITY MAPS AND INTENSITY CHANGE MAPS

The data set we use is the ANSS catalog of earthquakes [18] between latitude 32°N and 40°N and between longi-

BINARY FORECASTS

Binary forecasts are a well-known method for constructing forecasts of future event locations and have been widely used in tornado and severe storm forecast-

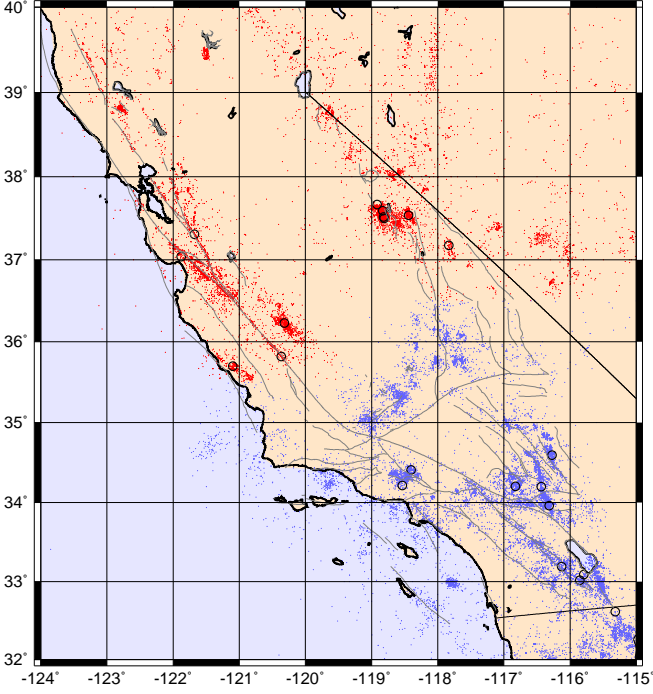


FIG. 1: Map of earthquake ($m \geq 3$) epicenters in California from 1932 to the present. Circles are events with $m \geq 6$ since 1960. Red epicenters define the area used to analyze seismicity in northern California; blue epicenters define the area used for southern California.

ing [15, 16]. We construct binary forecasts for $m \geq m_c$ and for times $t > t_2$, where m_c is a cutoff magnitude. In past work [13, 14, 15] we have taken $m_c = 5$, but we now remove this restriction. In our application, the probabilities $P_\mu \equiv P_\mu(\mathbf{x}, t_0, t_2)$ and $P_\Delta \equiv P_\Delta(\mathbf{x}, t_1, t_2)$ are converted to binary forecasts $B_\mu \equiv B_\mu(D, \mathbf{x}, t_0, t_2)$ and $B_\Delta \equiv B_\Delta(D, \mathbf{x}, t_1, t_2)$ by the use of a decision threshold D , where $D \in [0, \max\{P_\mu\}]$ or $D \in [0, \max\{P_\Delta\}]$ respectively [15, 16].

For a given value of D , we set $B_\mu = 1$ where $P_\mu > D$ and $B_\mu = 0$ otherwise. Similarly, we set $B_\Delta = 1$ where $P_\Delta > D$ and $B_\Delta = 0$ otherwise. The set of pixels $\{\mathbf{x}_\mu(D)\}$ where $B_\mu = 1$ and $\{\mathbf{x}_\Delta(D)\}$ where $B_\Delta = 1$ then constitute locations where future events $m \geq m_c$ are considered to be likely to occur. We call these locations *hotspots*. The locations where $B_\mu = 0$ and $B_\Delta = 0$ are sites where future events $m \geq m_c$ are unlikely to occur. In previous work, intensity maps and intensity change maps at a particular value of D were called *Relative Intensity* maps and *Pattern Informatics* maps. Examples of binary forecast maps are shown in Figure 2A.

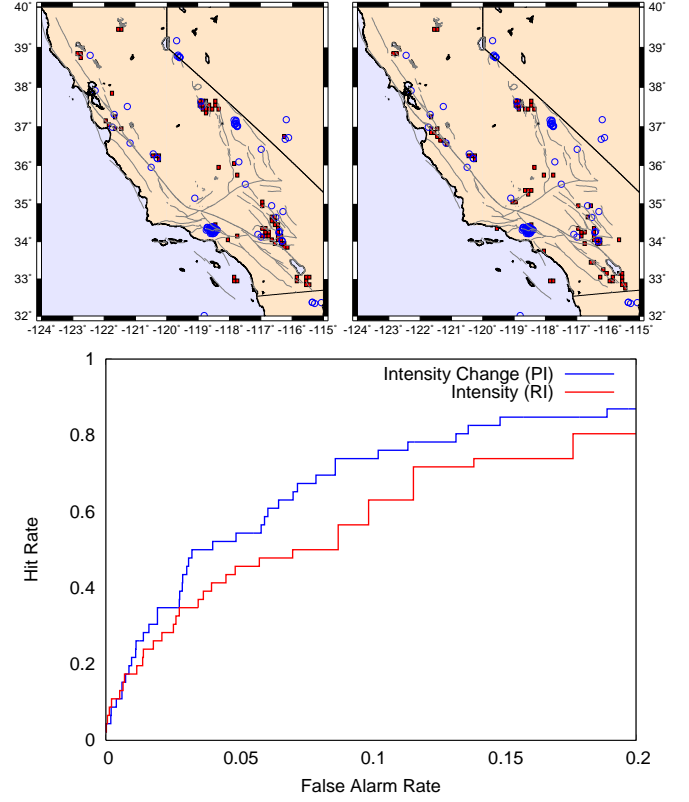


FIG. 2: (A) P_Δ (intensity change) map (left) and P_μ (average intensity) map (right). A decision threshold D was chosen leading to 75 hotspots in each map. Maps were computed for $t = 1$ December 1994 with $t_2 - t_1 = 13$ years. (B) ROC curves for P_Δ and P_μ corresponding to Figure 1. Here we have used $m_c = 4$.

RECEIVER OPERATING CHARACTERISTIC (ROC) DIAGRAMS

A series of D -dependent *contingency tables* are constructed using the set of locations $\{\mathbf{x}_q(m_c)\}$ where the $q = 1, \dots, Q$ large events $m \geq m_c$ are observed to actually occur during the forecast verification period $t > t_2$. The contingency table has 4 entries, $a \rightarrow d$, whose values are determined by some specified rule set [15, 16]. Here we use the following rules for given D (same rules for both “ μ ” and “ Δ ” subscripts):

1. a is the number of boxes in $\{\mathbf{x}(D)\}$ which are also in $\{\mathbf{x}_q(m_c)\}$
2. b is the number of boxes in $\{\mathbf{x}(D)\}$ whose location is not in $\{\mathbf{x}_q(m_c)\}$, i.e., is in the complement to $\{\mathbf{x}_q(m_c)\}$
3. c is the number of boxes in the complement to $\{\mathbf{x}(D)\}$ whose location is in $\{\mathbf{x}_q(m_c)\}$
4. d is the number of boxes in the complement to $\{\mathbf{x}(D)\}$ whose locations are in the complement to $\{\mathbf{x}_q(m_c)\}$

The *hit rate* is then defined as $H = a/(a + c)$, and the *false alarm rate* is defined as $F = b/(b + d)$. Note that with these definitions, $a + c = Q$, $a + b =$ number of hotspots, and $a + b + c + d = N$.

The ROC diagram [15, 16] is a plot of the points $\{H, F\}$ as D is varied. Examples of ROC curves corresponding to the intensity and intensity change maps in Figure 2A are shown in Figure 2B. A perfect *forecast of occurrence* (perfect order, no fluctuations) would consist of two line segments, the first connecting the points $(H, F) = (0, 0)$ to $(H, F) = (1, 0)$, and the second connecting $(H, F) = (1, 0)$ to $(H, F) = (1, 1)$. A curve of this type can be described as maximum possible hits ($H = 1$) with minimum possible false alarms ($F = 0$). Another type of perfect forecast (perfect order, no fluctuations) consists of two lines connecting the points $(0, 0)$ to $(0, 1)$ and $(0, 1)$ to $(1, 1)$, a perfect *forecast of non-occurrence*.

The line $H = F$ occupies a special status, and corresponds to a completely random forecast [15, 16] (maximum disorder, maximum fluctuations) where the false alarm rate is the same as the hit rate and no information is produced by the forecast. Alternatively, we can say that the *marginal utility* [17] of an additional hotspot, dH/dF , equals unity for a random forecast.

For a given time-dependent forecast $H(F, t)$, we consider the time-dependent *Pierce Skill Score* $H(F, t) - F$ [16], which measures the improvement in performance of $H(F, t)$ relative to the random forecast $H = F$. A *Pierce function* $\Psi(t)$ measures the area between $H(F, t)$ and the random forecast:

$$\begin{aligned}\Psi(t) &= \int_0^{F_{\max}} (H(F, t) - F) dF \\ &= A(t) - F_{\max}^2/2,\end{aligned}\quad (1)$$

where

$$A(t) = \int_0^{F_{\max}} H(F, t) dF. \quad (2)$$

The upper limit F_{\max} on the range of integration is a parameter whose value is set by the requirement that the marginal utility [17] of the forecast of occurrence $H(F, t)$ exceeds that of the random forecast $H = F$:

$$\frac{d}{dF} \{H(F, t) - F\} > 0. \quad (3)$$

Since $H(F, t)$ curves are monotonically increasing, F_{\max} is determined as the value of F for which $dH(F, t)/dF = 1$. For the forecasts we consider, we find that $F_{\max} \approx 0.2$, as can be seen from the examples in Figure 2B.

ORDER PARAMETER AND GENERALIZED GINZBURG CRITERION

We define an order parameter as the Pierce function $\Psi_\tau(t)$ obtained using as the probability $P_\tau \equiv$

$P_\tau(\mathbf{x}, t_1, t_2) = n(\mathbf{x}, t_1, t_2) / \int n(\mathbf{x}, t_1, t_2) d\mathbf{x}$, where P_τ is the average normalized intensity of seismic activity during t_1 to t_2 . Using P_τ and the decision threshold D , we construct a binary forecast $B_\tau \equiv B_\tau(D, \mathbf{x}, t_1, t_2)$. Evaluating the forecast B_τ during the time interval t_2 to t produces the ROC diagram $H_\tau(F, t)$. For the case of forecasts having positive marginal utility relative to the random forecast, $\Psi_\tau(t) > 0$. If past seismic activity is uncorrelated with future seismic activity, P_τ is equivalent to a random forecast, and $\Psi_\tau(t) = 0$.

Corresponding to the order parameter $\Psi_\tau(t)$, we define a function $\mathcal{G}(t)$ to indicate the relative importance of fluctuations with respect to forecasts of occurrence. We note that the probability Ψ_Δ is a measure of the mean squared change of intensity, a measure of fluctuations in seismic intensity, during t_1 to t_2 , and that the probability P_μ is a measure of the average intensity over the entire time history (t_0 to t_2). We will refer to P_Δ as the “fluctuation map” or “change map”, and P_μ as the “average map”.

Using the corresponding ROC functions we define

$$\mathcal{G}(t) \equiv \frac{\Psi_\Delta(t)}{\Psi_\mu(t)}, \quad (4)$$

where $\Psi_\Delta(t)$ is based upon the ROC curve computed using P_Δ , $\{H_\Delta(F, t), F\}$ and $\Psi_\mu(t)$ is based upon the ROC curve computed using P_μ , $\{H_\mu(F, t), F\}$. We can say that when $\mathcal{G}(t) < 1$, “fluctuations are less significant relative to the mean” in the sense that the fluctuation map provides a poorer forecast than the mean map. This statement is equivalent to the Pierce difference function:

$$\Delta A(t) \equiv A_\mu(t) - A_\Delta(t) > 0. \quad (5)$$

This difference function can be considered to be a *generalized Ginzburg criterion* [12].

To examine these ideas, we compare a plot of $\mathcal{G}(t)$ with activity of major earthquakes ($m \geq 6$) in California. We first consider the Gutenberg-Richter frequency-magnitude relation $f = 10^a \cdot 10^{-bm}$, where f is the number of events per unit time with magnitude larger than m and a and b are constants. a specifies the level of activity in the region, and $b \cong 1$.

To construct ROC curves, we consider t to be the current time at each time step and test the average map and change map by forecasting locations of earthquakes during t_2 to t . We use events having $m \geq m_T$, where m_T is some threshold magnitude. Note that f^{-1} specifies a time scale for events larger than m : 1 event with $m \geq 6.0$ is associated on average with 10 $m \geq 5.0$ events, 100 $m \geq 4.0$ events, etc. Without prior knowledge of the optimal value for m_T , we average the results for a scale-invariant distribution of 1000 $m_T \geq 3.0$ events, 794 $m_T \geq 3.1$ events, 631 $m_T \geq 3.2$ events, ..., 10 $m_T \geq 5.0$ events. We terminate the sequence at $m_T \geq 5.0$ due to increasingly poor statistics. To control the number of earthquakes with $m \geq m_T$ in the *snapshot window*

(t_2 to t), we determine the value of t_2 that most closely produces the desired number of events within the snapshot window. It is possible to have fluctuations in actual number of events if the snapshot window includes the occurrence time of a major earthquake, when there may be many events $m \geq m_T$ in the coarse-grained time intervals of length 1 day following the earthquake.

A central idea is that the length of the snapshot window is not fixed in time; it is instead fixed by earthquake number at each threshold magnitude $m_T = 3.0, 3.1, 3.2$, and so forth. Nature appears to measure “earthquake time” in numbers of events, rather than in years. “Earthquake time” is evidently based on stress accumulation and release, that is, earthquake numbers, rather than in months or years [10].

Results are shown in Figure 3 for the region of California shown in Figure 1. At top of either plot is the Pierce difference function $\Delta A(t) = A_\mu(t) - A_\Delta(t)$, and at bottom is earthquake magnitude plotted as a function of time from 1 January 1960 to 31 March 2006. The vertical lines in each top panel are the times of all events $m \geq 6$ in the region during that time interval. It can be seen from Figures 1 and 3 that there are 11 $m \geq 6$ events in northern California and 10 such events in southern California. For both areas, these major events are concentrated into 8 distinct “episodes” corresponding to 8 main shocks. In each plot, 7 of the 8 major episodes fall during (“black”) time intervals where $\Delta A(t) > 0$, or they either begin or terminate such a time interval. If a binomial probability distribution is assumed, the chance that random clustering of these major earthquake episodes could produce this temporal concordance can be computed. For Figure 3A, where black time intervals constitute 36.8% of the total, we compute a 0.46% chance that the concordance is due to random clustering. For Figure 3B, the respective numbers are 19% of the total time interval, and 0.0058% chance due to random clustering. Our results support the prediction that major earthquake episodes preferentially occur during time intervals when fluctuations in seismic intensity, as measured by ROC curves, are less important than the average seismic intensity.

This work has been supported by NASA Grant NGT5 to UC Davis (JRH), by a HSERC Discovery grant (KFT), by a US Department of Energy grant to UC Davis DE-FG03-95ER14499 (JRH and JBR), by a US Department of Energy grant to Boston University DE-FG02-95ER14498 (WK), and through additional funding from NSF grant ATM-0327558 (DLT).

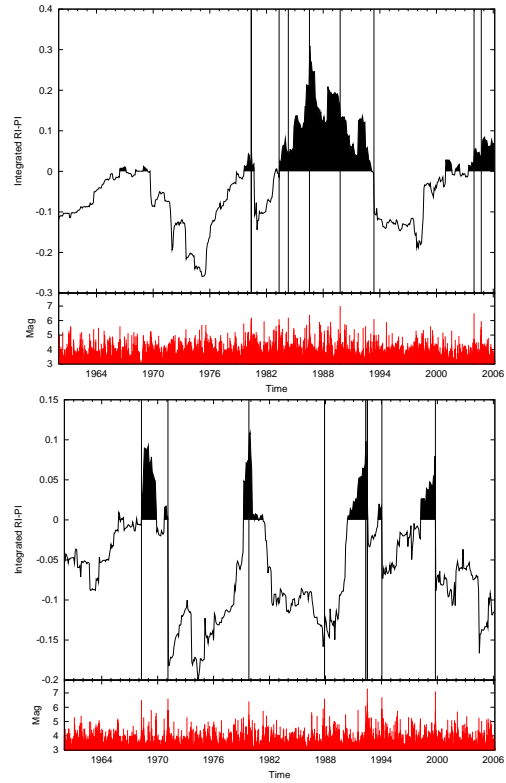


FIG. 3: Value of the Pierce difference function $\Delta A(t)$ (top) and magnitude (bottom) as a function of time for events occurring on the map area of Figure 1. Vertical black lines represent times of major earthquakes having $m \geq 6$ in the respective regions. Differences are computed for a scale-invariant distribution of magnitude thresholds in the snapshot window from $m_T = 3.0$ to $m_T = 5.0$. Area integration is performed for $F \in [0.0, 0.2]$. (A) Northern California (red epicenters in Figure 1). (B) Southern California (blue epicenters in Figure 1).

- [1] R. Burridge and L. Knopoff, *Bull. Seism. Soc. Am.* **57**, 341 (1967).
- [2] J. B. Rundle and D. D. Jackson, *Bull. Seism. Soc. Am.* **67**, 1363 (1977).
- [3] J. M. Carlson, J. S. Langer, and B. E. Shaw, *Rev. Mod. Phys.* **66**, 657 (1994).
- [4] I. G. Main and F. H. Al-Kindy, *Geophys. Res. Lett.* **108**, 2521 (2002).
- [5] K. Chen, P. Bak, and S. P. Obukhov, *Phys. Rev. A* **43**, 625 (1991).
- [6] D. L. Turcotte, *Fractals & Chaos in Geology & Geophysics* (Cambridge University Press, Cambridge, 1997), 2nd ed.
- [7] D. Sornette, *Critical Phenomena in the Natural Sciences* (Springer, Berlin, 2000).
- [8] D. S. Fisher, K. Dahmen, S. Ramanathan, and Y. Ben-Zion, *Phys. Rev. Lett.* **78**, 4885 (1997).
- [9] J. B. Rundle, W. Klein, and S. J. Gross, *Phys. Rev. Lett.* **76**, 4285 (1996).
- [10] W. Klein, J. B. Rundle, and C. D. Ferguson, *Phys. Rev. Lett.* **78**, 3793 (1997).
- [11] A. Helmstetter and D. Sornette, *J. Geophys. Res.* **107**, 2237 (2002).

* Electronic address: holliday@cse.ucdavis.edu

† Electronic address: jbrundle@ucdavis.edu

‡ Electronic address: turcotte@geology.ucdavis.edu

§ Electronic address: klein@physics.bu.edu

¶ Electronic address: ktiampo@seis.es.uwo.ca

- [12] N. Goldenfeld, *Lectures on Phase Transitions and the Renormalization Group* (Addison Wesley, Reading, MA, 1992).
- [13] J. B. Rundle, K. F. Tiampo, W. Klein, and J. S. S. Martins, Proc. Natl. Acad. Sci. U. S. A. **99**, 2514 (2002).
- [14] K. F. Tiampo, J. B. Rundle, S. McGinnis, S. J. Gross, and W. Klein, J. Geophys. Res. **107**, 2354 (2002).
- [15] J. R. Holliday, K. Z. Nanjo, K. F. Tiampo, J. B. Rundle, and D. L. Turcotte, Nonlinear Processes in Geophysics **12**, 965 (2005).
- [16] I. T. Jolliffe and D. B. Stephenson, *Forecast Verification* (John Wiley, Chichester, 2003).
- [17] J. W. Chung, *Utility and Production Functions* (Blackwell, Oxford, 1994).
- [18] <http://www.ncedc.org/cnss/>